THE ARCHIVE OF MECHANICAL ENGINEERING

VOL. LX 2013 Number 1

10.2478/meceng-2013-0008

Key words: perfectly elastic contact, perfectly plastic contact, optimal control, structure preserving simulation

MICHAEL W. KOCH [*], *SIGRID LEYENDECKER* [*]

STRUCTURE PRESERVING SIMULATION OF MONOPEDAL JUMPING

The human environment consists of a large variety of mechanical and biomechanical systems in which different types of contact can occur. In this work, we consider a monopedal jumper modelled as a three-dimensional rigid multibody system with contact and simulate its dynamics using a structure preserving method. The applied mechanical integrator is based on a constrained version of the Lagrange-d'Alembert principle. The resulting variational integrator preserves the symplecticity and momentum maps of the multibody dynamics. To ensure the structure preservation and the geometric correctness, we solve the non-smooth problem including the computation of the contact configuration, time and force instead of relying on a smooth approximation of the contact problem via a penalty potential. In addition to the formulation of non-smooth problems in forward dynamic simulations, we are interested in the optimal control of the monopedal high jump. The optimal control problem is solved using a direct transcription method transforming it into a constrained optimisation problem, see [14].

1. Introduction

A variety of biomechanical literature concerns the function and structure of the human locomotor system and often the focus is on walking movements [5, 17]. Here, we are interested in jumping movements as e.g. in [1]. The monopedal jumper is modelled as a constrained multibody body system and we simulate non-smooth forward dynamics and an optimal control problem. In contrast to rolling wheels, the locomotion with legs requires simulation techniques which handle the contact's establishing and releasing between the foot and the ground. The investigated contact formulation covers the theory of perfectly elastic and perfectly plastic contacts (e.g. see [8]), where the last

[*] *Chair of Applied Dynamics, University of Erlangen-Nuremberg, Konrad-Zuse-Straße 3/5, D-91052 Erlangen, Germany; E-mail: michael.koch@ltd.uni-erlangen.de, sigrid.leyendecker@ltd.uni-erlangen.de*

one means that the foot stays in contact with the ground for a certain time. The monopedal jumper model consists of an upper body representing the torso and the leg consists of two rigid bodies, which are connected at the knee joint. The inclusion of the knee joint leads to movements that differs from those considered e.g. in [7, 12], which are technically oriented jumpers. The forward dynamics simulations use a symplectic momentum integrator to compute the monopedal's motion and include the perfectly elastic and perfectly plastic contact formulations, which means that the relevant points in time when contact establishing and releasing takes place are determined. The optimally controlled jumper allows actuation in the hip and the knee joint, such that a physiologically motivated cost function is minimised. In the numerical solution, a direct transcription method is used to transform the optimal control problem into an optimisation problem being constrained by the fulfilment of discrete equations of motion, boundary conditions and path constraints, see e.g. [10, 18]. To avoid an artificial restriction of the optimisation problem by prescribing the time of contact establishing or release, variable time steps are used, wherefore two scaling parameters being part of the optimisation parameters are used.
Section 2 describes briefly the multibody formulation in redundant coordinates and introduces a corresponding actuation force formulation. The symplectic momentum integrator and the null space method with nodal reparametrisation, which reduces the numerical effort, are introduced in Section 3. Section 4 covers the optimal control problem and explains shortly the transfer into a finite dimensional optimisation problem. The simple monopedal jumper model is described in Section 5 and the discrete equations of motion corresponding to the perfectly elastic, respectively perfectly plastic contact for the variational approach are given in Section 6. In Section 7, the optimal control problem of high jumping is transformed into an optimisation problem with variable time step. Results for the forward dynamics as well as for the optimal control problem are presented in the corresponding sections.

2. Rigid multibody configuration and actuation

The simulation of multibody dynamics requires a description of the multibodies configuration – in this work we use the rotation free formulation introduced in [2] for rigid bodies and in [4] for rigid multibody systems. The α-th rigid body is specified by a configuration vector $\boldsymbol{q}^\alpha(t) \in \mathbb{R}^{12}$ composed by the placement of its center of mass $\boldsymbol{\varphi}^\alpha(t)$ and the right-handed director triad $\boldsymbol{d}_i^\alpha(t)$ for $i = 1, 2, 3$. The director triad specifies the body's orientation in space and has to stay orthonormal during the motion in the considered

time interval $[t_0, t_N]$, which is guaranteed by six so-called internal constraints $\boldsymbol{g}_{int}(\boldsymbol{q}^{\alpha}) = \boldsymbol{0} \in \mathbb{R}^6$.

In multibody systems, the rigid bodies are interconnected by different types of joints, e.g. revolute or spherical joints. The interconnection of the rigid bodies as well as their rigidity gives rise to a scleronomic and holonomic constraint function $\boldsymbol{g}(\boldsymbol{q}) \in \mathbb{R}^m$ on the redundant configuration variable $\boldsymbol{q} \in \mathbb{R}^k$, where k equals 12 times the number of bodies. The multibody systems are actuated directly by the independent generalised force $\boldsymbol{\tau} \in \mathbb{R}^{k-m}$ and the resulting k-dimensional redundant actuation $\boldsymbol{f}(\boldsymbol{q}) \in \mathbb{R}^k$ can be computed via $\boldsymbol{f}(\boldsymbol{q}) = \boldsymbol{B}^T(\boldsymbol{q}) \cdot \boldsymbol{\tau}$ with the input transformation matrix $\boldsymbol{B}^T(\boldsymbol{q}) \in \mathbb{R}^{k\times(k-m)}$. Note that the transformation matrix depends on the rigid bodies' interconnection and it is described in detail in [14].

3. Structure preserving integration for constrained mechanical systems

The dynamics of continuous mechanical systems can be described using the Lagrangian or Hamiltonian formalism. Here, discrete Lagrangian mechanics is used to derive a structure preserving integrator, see e.g. [16]. The constrained mechanical system is considered in a configuration manifold $Q \subseteq \mathbb{R}^k$ with the time-dependent configuration vector $\boldsymbol{q}(t) \in Q$. Corresponding to the approach in [14], the constrained version of the Lagrange-d'Alembert principle is discretised at the time nodes $\{t_0, t_1 = t_0 + \Delta t, \ldots, t_n = t_0 + n\Delta t, \ldots, t_N = t_0 + N\Delta t\}$, where $N \in \mathbb{N}$ is the number of time intervals and the discrete configurations $\boldsymbol{q}_n \approx \boldsymbol{q}(t_n)$ approximate the continuous trajectory. Similarly, $\boldsymbol{\lambda}_n \approx \boldsymbol{\lambda}(t_n)$ approximates the Lagrange multipliers with $\boldsymbol{\lambda}(t) \in \mathbb{R}^m$. As usual in the context of discrete variational mechanics, the discrete Lagrangian $L_d : Q \times Q \to \mathbb{R}$ is an approximation to the action integral of the continuous Lagrangian over one time-interval. The discrete Lagrange-d'Alembert principle requires stationarity of the resulting action sum, i.e.

$$\delta S_d = \delta \left[\sum_{n=0}^{N-1} L_d(\boldsymbol{q}_n, \boldsymbol{q}_{n+1}) - \frac{1}{2}(t_{n+1} - t_n) \left[\boldsymbol{g}^T(\boldsymbol{q}_n) \cdot \boldsymbol{\lambda}_n - \boldsymbol{g}^T(\boldsymbol{q}_{n+1}) \cdot \boldsymbol{\lambda}_{n+1} \right] \right] + \sum_{n=0}^{N-1} \boldsymbol{f}_n^- \cdot \delta \boldsymbol{q}_n + \boldsymbol{f}_n^+ \cdot \delta \boldsymbol{q}_{n+1} = \boldsymbol{0}$$

for all variations $\delta\boldsymbol{q}_n$ and $\delta\boldsymbol{\lambda}_n$. This leads to the $(k + m)$-dimensional constrained forced discrete Euler-Lagrange equations

$$D_2 L_d(\boldsymbol{q}_{n-1}, \boldsymbol{q}_n) + D_1 L_d(\boldsymbol{q}_n, \boldsymbol{q}_{n+1}) - \boldsymbol{G}_d^T(\boldsymbol{q}_n) \cdot \boldsymbol{\lambda}_n + \boldsymbol{f}_{n-1}^+ + \boldsymbol{f}_n^- = \boldsymbol{0} \quad (1)$$

$$\boldsymbol{g}(\boldsymbol{q}_{n+1}) = \boldsymbol{0}, \quad (2)$$

for $n = 1, \ldots, N-1$. Here $\boldsymbol{G}_d = \frac{1}{2}(t_{n+1} - t_{n-1})\frac{\partial \boldsymbol{g}}{\partial \boldsymbol{q}_n}$ denotes the $(m \times k)$-dimensional Jacobian matrix of the constraints, and $\boldsymbol{f}_n^- = \frac{1}{2}(t_{n+1} - t_n)\boldsymbol{B}^T(\boldsymbol{q}_n) \cdot \boldsymbol{\tau}_n$, respectively $\boldsymbol{f}_{n-1}^+ = \frac{1}{2}(t_n - t_{n-1})\boldsymbol{B}^T(\boldsymbol{q}_n) \cdot \boldsymbol{\tau}_{n-1}$ are called left and right discrete forces. The resulting mechanical integrator represents exactly the behaviour of the analytical system concerning the consistency of the momentum maps and symplecticity. Due to these preservation properties it is called symplectic momentum scheme. A further benefit of this mechanical integrator is the good energy behaviour, which means that there is no numerical gaining or dissipation of energy.

According to [3, 4], we apply the discrete null space method to reduce the dimension of the constrained forced discrete Euler-Lagrange equations. The discrete null space matrix $\boldsymbol{P} \in \mathbb{R}^{k \times (k-m)}$ fulfils the property $\boldsymbol{G}_d \cdot \boldsymbol{P} = \boldsymbol{0}$ and if we premultiply Equation (1) by the transposed null space matrix, then the constraint forces and thereby the Lagrange multipliers vanish. The resulting k-dimensional system is called reduced forced discrete Euler-Lagrange equations. The minimal dimension of the system can be achieved using the vector of incremental generalised coordinates $\boldsymbol{u}_{n+1} \in U \subset R^{(k-m)}$ to reparametrise the configuration vector $\boldsymbol{q}_{n+1}$ in the neighbourhood of $\boldsymbol{q}_n$. The nodal reparametrisation function $\boldsymbol{F}_d : U \times Q \to Q$

$$\boldsymbol{q}_{n+1} = \boldsymbol{F}_d(\boldsymbol{u}_{n+1}, \boldsymbol{q}_n) \tag{3}$$

fulfils the constraint conditions and therefore Equation (2) becomes unnecessary. Finally, the number of unknowns and thereby numerical effort is reduced by the formulation in discrete generalised coordinates $\boldsymbol{u}_d = \{\boldsymbol{u}_n\}_{n=0}^{N}$ and the discrete torques $\boldsymbol{\tau}_d = \{\boldsymbol{\tau}_n\}_{n=0}^{N-1}$. The dimension of the equations of motion is reduced to $k - m$.

$$\boldsymbol{P}^T(\boldsymbol{q}_n) \cdot \Big[D_2 L_d(\boldsymbol{q}_{n-1}, \boldsymbol{q}_n) + D_1 L_d(\boldsymbol{q}_n, \boldsymbol{F}_d(\boldsymbol{u}_{n+1}, \boldsymbol{q}_n)) + \boldsymbol{f}_{n-1}^+(\boldsymbol{q}_n, \boldsymbol{\tau}_{n-1}) + \boldsymbol{f}_n^-(\boldsymbol{q}_n, \boldsymbol{\tau}_n) \Big] = \boldsymbol{0} \tag{4}$$

4. Optimal control problem

In general, the goal of optimal control problems is to determine the optimal state trajectory and force field for the – in our case holonomically constrained systems, which move from the initial state $\boldsymbol{q}(t_0) = \boldsymbol{q}_0$, $\dot{\boldsymbol{q}}(t_0) = \dot{\boldsymbol{q}}_0$

to a final state $\boldsymbol{q}(t_N) = \boldsymbol{q}_N$, $\dot{\boldsymbol{q}}(t_N) = \dot{\boldsymbol{q}}_N$. The investigated system fulfils the equations of motion and at the same time the objective functional

$$J(\boldsymbol{q}, \dot{\boldsymbol{q}}, \boldsymbol{f}) = \int_{t_0}^{t_N} C(\boldsymbol{q}, \dot{\boldsymbol{q}}, \boldsymbol{f})\, dt$$

is minimised, where the integrand $C(\boldsymbol{q}, \dot{\boldsymbol{q}}, \boldsymbol{f}) : TQ \times T^*_q Q \to \mathbb{R}$ is a given cost function. The optimal control problem is solved using a direct transcription method, which transforms it into a constrained optimisation problem. The discrete objective function approximates the integral of the continuous cost function and the discrete constrained optimisation problems reads

$$\min_{\boldsymbol{u}_d, \boldsymbol{\tau}_d} \overline{J}(\boldsymbol{u}_d, \boldsymbol{\tau}_d) = \min_{\boldsymbol{u}_d, \boldsymbol{\tau}_d} \sum_{n=0}^{N-1} \overline{C}(\boldsymbol{u}_n, \boldsymbol{u}_{n+1}, \boldsymbol{\tau}_n), \tag{5}$$

subject to the constraints given by the reduced discrete equations of motion of the symplectic momentum scheme in Equation (4). In addition to the discrete equations of motion of the specific mechanical integrator, further constraints, like initial conditions, final conditions and possible inequality path constraints can be imposed.

5. Monopedal jumper

The three-dimensional model of the monopedal jumper is inspired by the human locomotor system. The characteristics of jumping are analysed using a reduced system of three rigid bodies, which represents the calf, thigh and upper part of the body, see Figure 1.

The human knee joint is modelled as a revolute joint, where the unit vector $\boldsymbol{n}_1$ in body 2 specifies the axis of rotation and the hip is modelled by a spherical joint. Note, that in reality the possible angles of anatomical joints are restricted, accordingly, in case of the optimal control problem, an inequality constraint function $h_{3d}(\boldsymbol{q}) < 0$ prevents the human knee's super-extension and as a result of this, the angle between thigh and calf is smaller than π. The motion of the upper part of the body is supported by a prismatical joint, i.e. only translation parallel to the $\boldsymbol{e}_3$-direction is allowed. The constrained system of the monopedal jumper is described by a 36-dimensional configuration variable and due to the rigidity $m_{int} = 18$ internal constraints are present. The joint interconnections cause $m_{ext} = 13$ external constraints and therefore the model is restricted by $m = 31$ holonomic constraints. Cor-

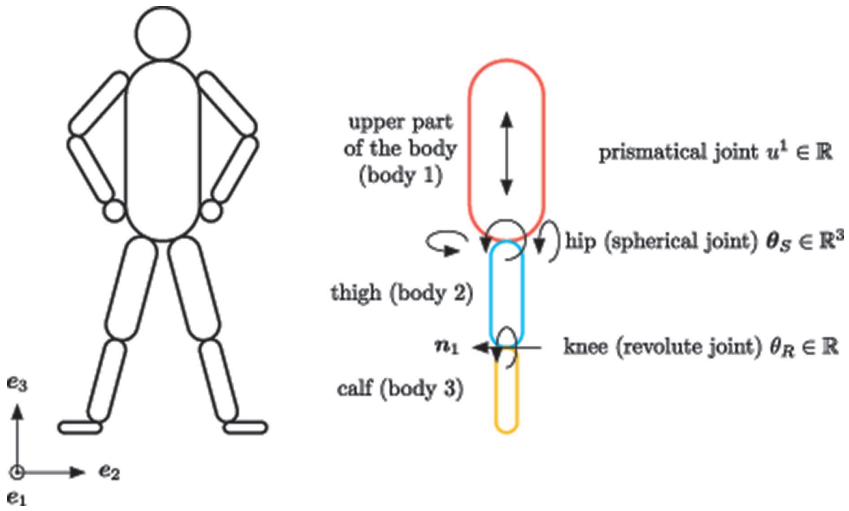

Fig. 1. Model of the three-dimensional jumper and its generalised coordinates

responding to the $k - m = 5$ degrees of freedom, the generalised coordinates and actuations read

$$\boldsymbol{u} = \begin{bmatrix} u^1 \\ \boldsymbol{\theta}_S \\ \theta_R \end{bmatrix} \in \mathbb{R}^5 \qquad \text{and} \qquad \boldsymbol{\tau} = \begin{bmatrix} \tau^1 \\ \boldsymbol{\tau}_S \\ \tau_R \end{bmatrix} \in \mathbb{R}^5 \tag{6}$$

with the translational motion $u^1 \in \mathbb{R}$ and force $\tau^1 \in \mathbb{R}$ in $\boldsymbol{e}_3$-direction. The vector $\boldsymbol{\theta}_S \in \mathbb{R}^3$ represents the relative rotation in the hip and $\theta_R \in \mathbb{R}$ the relative rotation of the calf (see Figure 1 for details). The monopedal jumper's hip is actuated by the torques $\boldsymbol{\tau}_S \in \mathbb{R}^3$ and $\tau_R \in \mathbb{R}$ acts at the knee joint.

6. Contact formulation

Within the forward dynamics simulation of the monopedal jumper, the theory of perfectly elastic and perfectly plastic contacts are discussed. The latter one means that the jumper's foot sticks to the ground as long as the contact force prevents the penetration of the ground. As soon as the contact force is zero, the foot should be released since when its sign changes, it would prevent the foot from lifting which is not consistent with the model of a foot ground contact during a jump.

6.1. Perfectly Elastic Contact Formulation

The simulation of perfectly elastic contacts using a variational integrator is performed for chains of point masses in a box in [15] and further detail can also be found in [6]. Here, the implemented non-penetration condition $g_c(\boldsymbol{q}) \geq 0 \in \mathbb{R}$ specifies the distance between the foot and the ground, whereby the ground is the $(\boldsymbol{e}_1, \boldsymbol{e}_2)$-plane (see Figure 2).
As long as the non-penetration condition is not violated, the forward dynamics simulation computes a new configuration $\boldsymbol{q}_{n+1}$ using a constant time step Δt in the discrete Euler-Lagrange equations in Equation (1-2). After every time step, the fulfilment of the inequality constraint is checked for the new configuration $\boldsymbol{q}_{n+1}$. If it is violated, i.e. $g_c(\boldsymbol{q}_{n+1}) < 0$, then the configuration $\boldsymbol{q}_{n+1}$ is discarded (see e.g. dashed configuration in Figure 2), and the physically correct contact configuration $\boldsymbol{q}_\iota$ must be calculated.

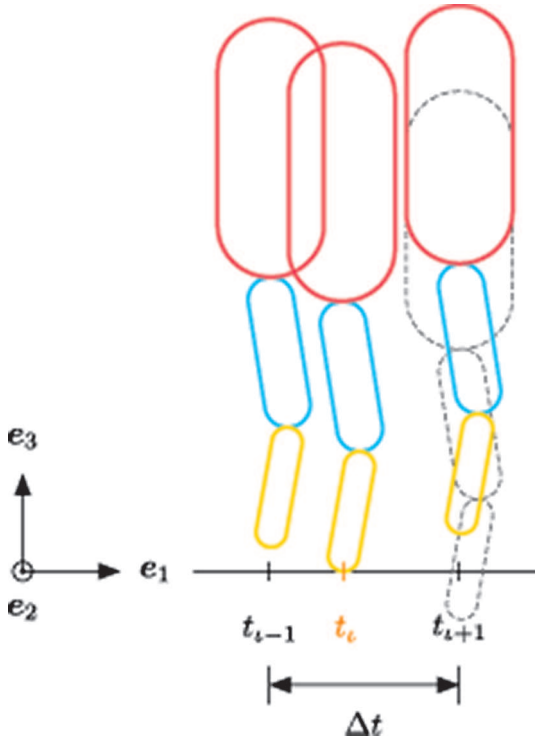

Fig. 2. Perfectly elastic contact

Table 1.
Physical quantities of the calf, thigh (taken from [19]) and the human torso (taken from [9] with a total weight of 64.90 $[kg]$)

physical quantity	**calf**	**thigh**	**torso**
mass $[kg]$	3.2800	6.8600	28.2055
moment of inertia $[kgm^2]$			
$I_{e_1e_1}$	0.0490	0.1238	0.1368
$I_{e_2e_2}$	0.0504	0.1188	0.1368
$I_{e_3e_3}$	0.0037	0.0229	0.9035

The contact configuration $\boldsymbol{q}_\iota$, the time of contact t_ι and the Lagrange multipliers $\boldsymbol{\lambda}_{\iota-1}$ are determined by solving the $(k+m+1)$ equations

$$D_2L_d(\boldsymbol{q}_{\iota-2},\ \boldsymbol{q}_{\iota-1}) + D_1L_d(\boldsymbol{q}_{\iota-1},\ \boldsymbol{q}_\iota, t_{\iota-1}, t_\iota) - \boldsymbol{G}_d^T(\boldsymbol{q}_{\iota-1})\cdot\boldsymbol{\lambda}_{\iota-1} + \boldsymbol{f}_{\iota-2}^+ + \boldsymbol{f}_{\iota-1}^- = \boldsymbol{0} \tag{7}$$

$$\boldsymbol{g}(\boldsymbol{q}_\iota) = \boldsymbol{0} \tag{8}$$

$$g_c(\boldsymbol{q}_\iota) = 0. \tag{9}$$

Equation (9) describes the contact condition, which is needed to compute the contact time t_ι. In the following time interval, $\boldsymbol{q}_{\iota+1}$, $\boldsymbol{\lambda}_\iota$ and the contact force Lagrange multiplier λ_c follow from

$$\begin{aligned} &D_2L_d(\boldsymbol{q}_{\iota-1},\ \boldsymbol{q}_\iota, t_{\iota-1}, t_\iota) + D_1L_d(\boldsymbol{q}_\iota,\ \boldsymbol{q}_{\iota+1}, t_\iota, t_{\iota+1}) \\ &\qquad -\boldsymbol{G}_d^T(\boldsymbol{q}_\iota)\cdot\boldsymbol{\lambda}_\iota - (\boldsymbol{G}_c^T)_d(\boldsymbol{q}_\iota)\cdot\lambda_c + \boldsymbol{f}_{\iota-1}^+ + \boldsymbol{f}_\iota^- = \boldsymbol{0} \\ &\qquad\qquad \boldsymbol{g}(\boldsymbol{q}_{\iota+1}) = \boldsymbol{0} \\ &D_4L_d(\boldsymbol{q}_{\iota-1},\ \boldsymbol{q}_\iota, t_{\iota-1}, t_\iota) + D_3L_d(\boldsymbol{q}_\iota,\ \boldsymbol{q}_{\iota+1}, t_\iota, t_{\iota+1}) = 0, \end{aligned} \tag{10}$$

where Equation (10) is a conservation condition for the discrete energy being the essential property of a perfect elastic contact.

6.1.1. Numerical Example

The conservation of energy is an essential feature of the perfectly elastic contact formulation. To demonstrate the energy's long term behaviour, we consider an example with a straight leg. The physical parameters of the torso, calf and the thigh are listed in Table 1. The motion starts at rest and the position of the calf's center of mass is given by $\boldsymbol{\varphi}_0^3 = [0, 0, 0.5]\ m$. We simulate

a time interval of 400 s and therein more than 830 contacts are counted. The algorithm's long term energy behaviour is plotted in Figure 3 and it shows a slight oscillation of the total energy (as it is typical for variational integrators), but the algorithm does not dissipates energy numerically. More details on the perfectly elastic contact formulation and another example are given in [11].

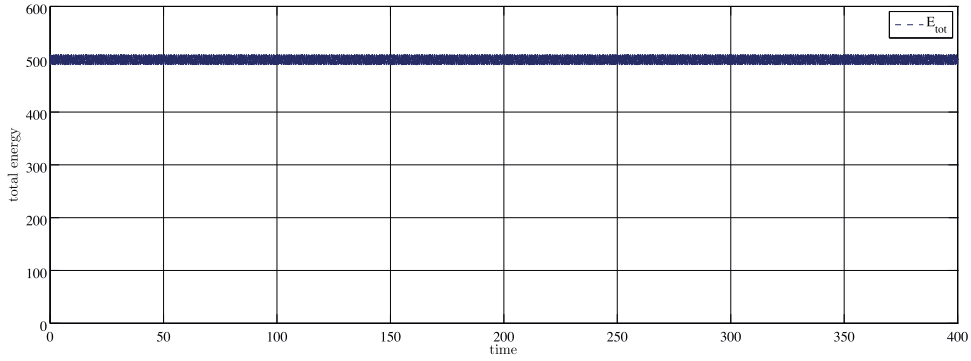

Fig. 3. Energy evolution for 830 contacts

6.2. Perfectly Plastic Contact Formulation

In case of the perfectly plastic contact, the jumper's foot stays in contact to the ground for a certain time and the contact is released as soon as the contact force in $\boldsymbol{e}_3$-direction changes its algebraic sign, since this would mean the foot is prevented from lifting off the ground. During the flight phase ($g_c > 0$), the forward dynamics simulation computes a new configuration $\boldsymbol{q}_{n+1}$ using a constant time step Δt. Analogue to the perfectly elastic contact, the configuration $\boldsymbol{q}_{n+1}$ is checked after every time step and if the non-penetration condition is violated, then the Equations (7-9) are used to determine the time and configuration of contact establishing. While the contact stays closed, the foot is fixed at the ground in $\boldsymbol{x}_S$ by a spherical joint. The corresponding constraint reads $\boldsymbol{g}_S(\boldsymbol{q}_n) = \boldsymbol{\varphi}_n^3 + \boldsymbol{\varrho}_n^3 - \boldsymbol{x}_S = \boldsymbol{0} \in \mathbb{R}^3$ and the resulting contact force is computed as $\boldsymbol{f}_S(\boldsymbol{q}) = \boldsymbol{G}_S^T(\boldsymbol{q}) \cdot \boldsymbol{\lambda}_S \in \mathbb{R}^{36}$. For $t_n > t_\iota$, the contact configurations $\boldsymbol{q}_n$, the Lagrangian multipliers $\boldsymbol{\lambda}_{n-1}$ and $\boldsymbol{\lambda}_{S_{n-1}}$ are determined by solving the $(k + m + 3)$-dimensional system of equations

$$D_2L_d(\boldsymbol{q}_{n-1}, \boldsymbol{q}_n) + D_1L_d(\boldsymbol{q}_n, \boldsymbol{q}_{n+1}) - \boldsymbol{G}_d^T(\boldsymbol{q}_n) \cdot \boldsymbol{\lambda}_n - (\boldsymbol{G}_S^T)_d(\boldsymbol{q}_n) \cdot \boldsymbol{\lambda}_{S_n} + \boldsymbol{f}_{n-1}^+ + \boldsymbol{f}_n^- = \boldsymbol{0} \tag{11}$$

$$\boldsymbol{g}(\boldsymbol{q}_{n+1}) = \boldsymbol{0}$$

$$\boldsymbol{g}_S(\boldsymbol{q}_{n+1}) = \boldsymbol{0}.$$

The contact force vector $\boldsymbol{f}_S$ immobilises the jumper's foot in $\boldsymbol{x}_S$ and its function is to prevent the penetration of the ground, thereby the third component of the Lagrange multiplier is negative ($\lambda^3_{S_n} < 0$). If $\lambda^3_{S_n} > 0$, the contact force would prevent the foot from lifting of the ground. When this happens, the current configuration is discarded (see the right dashed configuration in Figure 4). The violation of this condition implies, that during the constant time-step the foot would release the contact with the ground, but this is artificially prevented by the force vector $\boldsymbol{f}_S$.

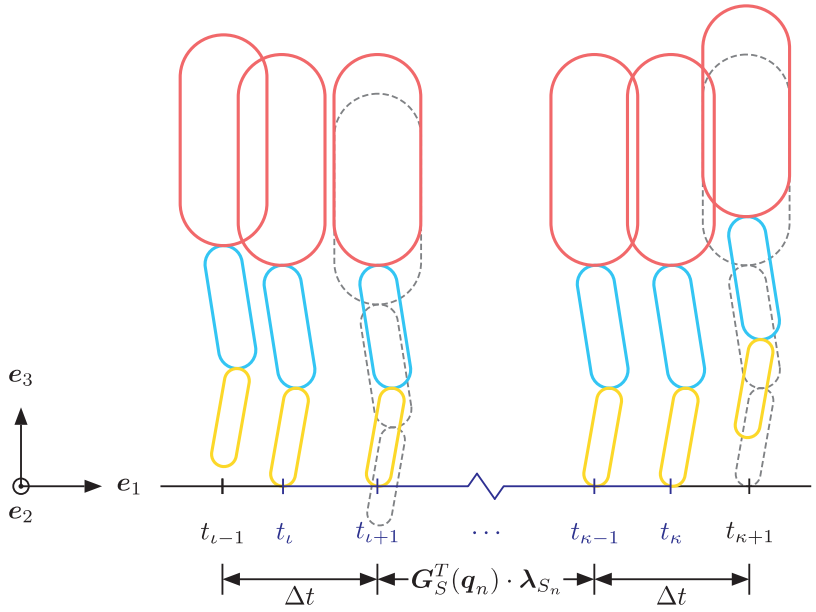

Fig. 4. Perfectly plastic contact

Therefore, the last contact configuration $\boldsymbol{q}_\kappa$, the time of contact release t_κ, the internal and external Lagrange multipliers and the contact multipliers are determined by solving the $(k + m + 3 + 1)$ equations

$$\begin{aligned} D_2L_d(\boldsymbol{q}_{\kappa-2}, \boldsymbol{q}_{\kappa-1}) + D_1L_d(\boldsymbol{q}_{\kappa-1}, \boldsymbol{q}_\kappa) \\ -\boldsymbol{G}_d^T(\boldsymbol{q}_{\kappa-1}) \cdot \boldsymbol{\lambda}_{\kappa-1} - (\boldsymbol{G}_S^T)_d(\boldsymbol{q}_{\kappa-1}) \cdot \boldsymbol{\lambda}_{S_{\kappa-1}} + \boldsymbol{f}^+_{\kappa-2} + \boldsymbol{f}^-_{\kappa-1} &= \boldsymbol{0} \\ \boldsymbol{g}(\boldsymbol{q}_\kappa) &= \boldsymbol{0} \\ \boldsymbol{g}_S(\boldsymbol{q}_\kappa) &= \boldsymbol{0} \\ \lambda^3_{S_{\kappa-1}} &= 0. \end{aligned} \tag{12}$$

Equation (12) is necessary to compute the point in time, at which the foot releases the contact with the ground. The forward dynamics after the contact release is described again by the Equations (1) - (2).

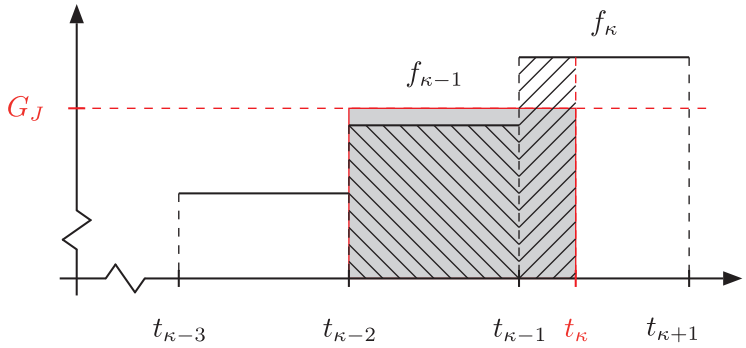

Fig. 5. Determination of the contact release time for the upright monopedal jumper

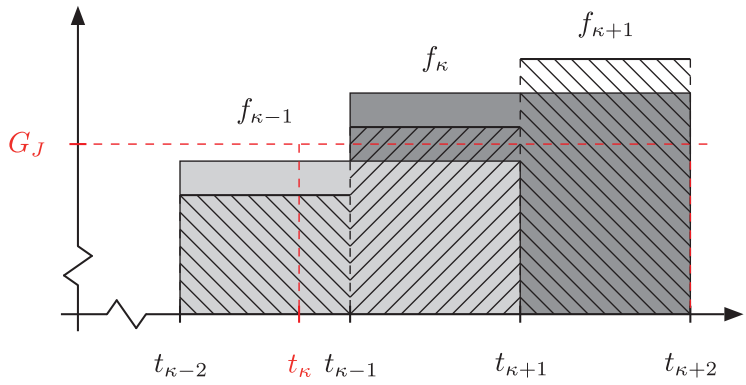

Fig. 6. Determination of a non-physical backward time step for the upright monopedal jumper

The determination of the contact release time can be a difficult task. For simplicity, let us consider the special case when the jumper is standing on the ground at rest in an upright position. The jumper is actuated by translational forces $f_{n-1},\ f_n \in \mathbb{R}$ at the upper part of the body and the forces act in the jumpers longitudinal direction. At the contact release time, the actuation force is in equilibrium with the gravitational force of the total body. However, in the context of the discrete forced Euler-Lagrange equations, the force equilibrium depends on the time step, in particular it reads

$$(t_\kappa - t_{\kappa-2})G_J = (t_{\kappa-1} - t_{\kappa-2})f_{\kappa-1} + (t_\kappa - t_{\kappa-1})f_\kappa, \tag{13}$$

whereby G_J represents the gravitational force. The monopedal jumper releases the contact as soon as the integral of the actuation forces $f_{\kappa-1}$ and f_κ is equal to the integral of the jumper's gravity force. Therefore, we investigate two different cases. The first one is illustrated in Figure 5, here, the actuation force $f_{\kappa-1}$ is smaller but f_κ is greater than G_J. Due to that, the temporal average of the actuation is greater than the jumper's weight and therefore the algorithm computes a correct time node $t_\kappa > t_{\kappa-1}$ for the contact release

(see the grey shaded area in Figure 5). The other case is illustrated in Figure 6, where the force function is approximated by an other step function. In this situation a non-physical contact release time is determined, because the temporal average of the actuation forces $f_{\kappa-1}$ and f_κ (see the light grey shaped area) is smaller than the gravitational forces and at the next step, both actuation forces are greater than the G_J and so a negative time step ($t_\kappa < t_{\kappa-1}$) is the result of the forward dynamics simulation. If this happens, the contact release time interval is subdivided, thus the approximation to the actuation is refined until a physically meaningful contact release time is found. In this work, we examine two strategies to refine the approximation of the jumper's actuation. In Figure 7a), the contact release time interval is subsequently divided in the middle (bisection) until a physical contact release time is computed. The second possibility is illustrated in Figure 7b), where the initial contact release interval is subdivided in $p \in \mathbb{N}$ equal subintervals of time step $\frac{1}{p}\Delta t$, and p increases until a physical correct release time is computed.

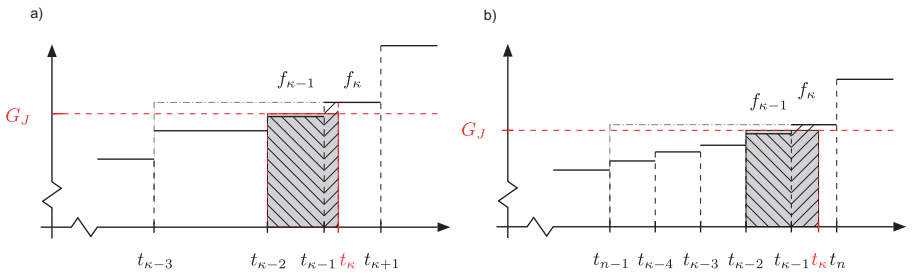

Fig. 7. Determination of the contact release time for the monopedal jumper using the subdivision with a subsequent bisection in a) and with increasing number of p subintervals (here $p = 5$) in b)

6.2.1. Numerical Examples

This section illustrates the properties of the perfectly plastic contact formulation considering the different strategies to determine a physical correct time of the contact release. The jumper's motion starts at rest with a straight leg and the foot is in contact with the ground in $\boldsymbol{x}_S = [0, 0, 0]\ m$. The upper part of the body is actuated by a force approximated by a monotonously increasing step function and the discrete equations of motion are solved using the Newton-Raphson method with an numerical accuracy of 10^{-8}.

At first, we investigate an example, in which no refinement strategy needs to be used to compute the physically correct contact release time. In this case, a basis time step of $\Delta t = 0.015\ s$ is used and the applied step function

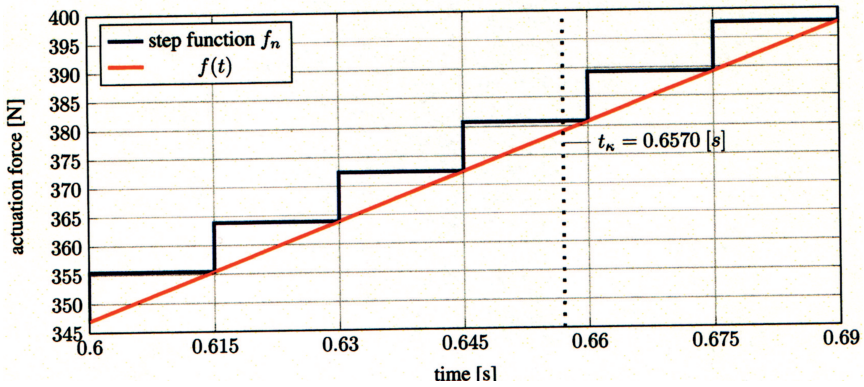

Fig. 8. Visualisation of the continuos actuation function and the implemented step function

evaluates the continuous function $f(t) = \frac{3}{2}G_J(t + 0.015)$ at the right side of each time interval. The resulting step function is a rough approximation of the continuos actuation force $f(t)$. Figure 8 illustrates the continuous function and the step function f_n and it also depicts the computed contact release time at $t_\kappa = 0.6570\ s$.

The next example illustrates the properties of the two introduced refinement strategies. Both strategies are implemented with a basic time step of $\Delta t = 0.0075\ s$ and the upper part of the body is actuated by a monotonously increasing step function, which evaluates the continuous function $f(t) = \frac{3}{2}G_J(t + 0.0075)$.

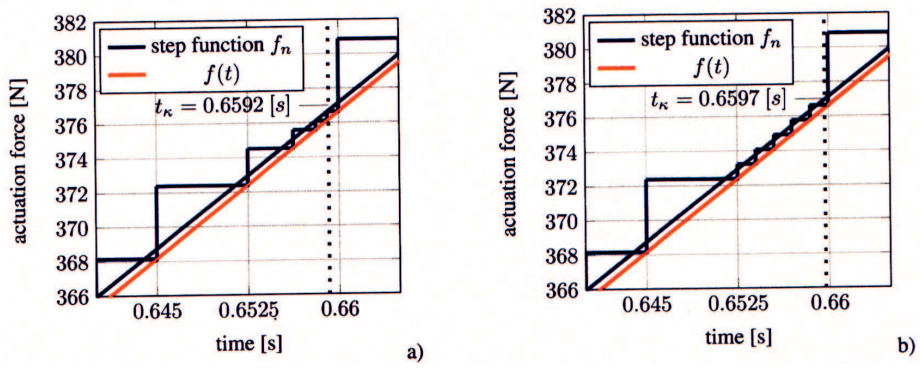

Fig. 9. Visualisation of both possibilities to determine the correct contact release time for the monopedal jumper. In a) the bisection approximation is used three times and in b) the basis time step is subdivided in $p = 5$ subintervals

According to Equation (13), the time of contact release is expected in the time interval $[0.6525, 0.66]\ s$. The first refining algorithm uses three bisections to determine the time of contact release at $0.6592\ s$. The second

possibility subdivides the standard time step into 5 subintervals and computes the time of contact release at 0.6597 s. The small disparity between the contact release times is a result of the different refinement strategies.

7. Optimal control of the monopedal jumper

The goal of the optimal control problem is to find the optimal state trajectory and the optimal control sequence leading the jumper from an initial to a final state. In contrast to the aforementioned examples, here, the jumper is actuated in the hip and in the knee joint only. The optimal control problem starts at rest and the foot is in contact with the ground, which is modelled as a perfectly plastic contact. As it is illustrated in Figure 10, the optimal control problem considers a motion with a contact and a flight phase, whereby the maximum jump height is required at the end of the flight phase.

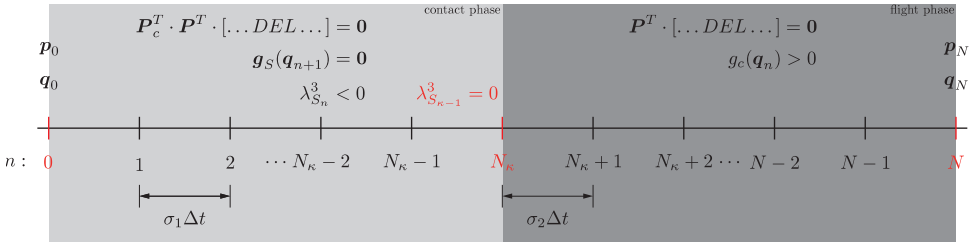

Fig. 10. Time grid and dynamical constraints of the jumpers's optimal control problem

The constrained optimisation problem is formulated in terms of the discrete generalised coordinates $\boldsymbol{u}_d$ and actuations $\boldsymbol{\tau}_d$ corresponding to Equation (6). During the flight phase, the dynamical constraints are given by Equation (4) which is a 5-dimensional system of equations. In the context of the optimal control problem, also the contact phase at the beginning of the manoeuvre needs to be described using discrete equations of motion of minimal dimension, thus here, the dimension of Equation (11) needs to be reduced. Analoguous to the procedure during the flight phase, here the $(k+m+3)$-dimensional forced discrete Euler-Lagrange equations are premultiplied by the contact null space matrix $\boldsymbol{P}_c(\boldsymbol{q}_n) \in \mathbb{R}^{5\times 2}$ and by the null space matrix $\boldsymbol{P}(\boldsymbol{q}_n) \in \mathbb{R}^{36\times 5}$, such that the constraint forces and also the contact forces vanish (see Equation (14)). A further reduction is achieved by applying the nodal reparametrisation of the flight phase $\boldsymbol{F}_d$ from Equation (3) (fulfilling the constraints $\boldsymbol{g}(\boldsymbol{q}_{n+1}) = \mathbf{0}$ in Equation (11)). Thus, the forced discrete equations of motion during the contact phase are also reduced to a 5-dimensional system. At this point it should be mentioned, that during the contact phase, the discussed monopedal jumper has two degrees of freedom. However, a maximal reduction would require a new nodal reparametrisation

which is highly nonlinear (involving trigonometric functions). Experience has shown that it is easier and faster for the optimiser to work with a slightly larger number of dynamical constraints being less nonlinear.

In case of the forward dynamics simulation, the contact force prevents the penetration of the ground and as soon as the contact force changes its algebraic sign, the algorithm computes a contact release time and configuration. During the contact phase of the optimal control problem, inequality path constraints guarantee the correct orientation of the contact force, i.e. the correct sign of the Lagrange multiplier $\lambda^3_{S_n} < 0$ for $n = 1, \ldots, \kappa - 2$. However, due to the premultiplication by the contact null space matrix $\boldsymbol{P}_c(\boldsymbol{q}_n)$, the contact force is eliminated from Equation (14). Thus, the corresponding Lagrange multiplier must be recalculated after every time step to be able to check whether it has the correct sign meaning that it fulfils the inequality path constraints of the optimal control problem during the contact phase. The contact Lagrange multipliers can be calculated via

$$\boldsymbol{\lambda}_{S_n} = \boldsymbol{S}^T(\boldsymbol{q_n}) \cdot \boldsymbol{P}^T(\boldsymbol{q}_n) \cdot \left[D_2 L_d(\boldsymbol{q}_{n-1}, \boldsymbol{q}_n) + D_1 L_d(\boldsymbol{q}_n, \boldsymbol{q}_{n+1}) + \boldsymbol{f}^+_{n-1} + \boldsymbol{f}^-_n \right],$$

$$\text{with} \quad \boldsymbol{S}(\boldsymbol{q_n}) = \boldsymbol{P}^T(\boldsymbol{q}_n) \cdot \boldsymbol{G}_S^T(\boldsymbol{q}_n) \cdot \left(\boldsymbol{G}_S(\boldsymbol{q}_n) \cdot \boldsymbol{P}(\boldsymbol{q}_n) \cdot \left[\boldsymbol{G}_S(\boldsymbol{q}_n) \cdot \boldsymbol{P}(\boldsymbol{q}_n) \right]^T \right)^{-1} \in \mathbb{R}^{5\times 3}.$$

The boundary conditions $\boldsymbol{h}_{1d}(\boldsymbol{q}_0, \boldsymbol{p}_0) = \boldsymbol{0} \in \mathbb{R}^2$ guarantee an initial state $\boldsymbol{q}(t_0) = \boldsymbol{q}^0$, $\boldsymbol{p}(t_0) = \boldsymbol{p}^0$ of the jumper, whereby $\boldsymbol{p}^0 \in \mathbb{R}^{36}$ represents the conjugate momentum at the initial configuration. In this first example, a path constraint function $h_{2d}(\boldsymbol{q}_n) = 0$ is used to restrict the jumping movement into the $(\boldsymbol{e}_1, \boldsymbol{e}_3)$-plane and therefore the jumper is only actuated by torques in the $\boldsymbol{e}_2$-direction. The actuation of the monopedal jumper during the contact phase has an essential effect on the time of release and on the height of the jump. The optimal contact release time is not known a priori, it is part of the optimal control problem. To realise this in the implementation, the node number N_κ of the contact release time node t_{N_κ} is predefined, but the physical time t_{N_κ} itself is an unknown which has to be determined by the optimisation. Thus, the time steps before and after the contact release time are scaled by the parameters $\sigma_1,\ \sigma_2 \in \mathbb{R}$ (see Figure 10) and these scalars are part of the optimisation variables. Finally, the constrained optimisation problem of the monopedal jumpers reads

$$\min_{\boldsymbol{u_d}, \boldsymbol{\tau}_d, \sigma_1, \sigma_2} \tilde{J}_d(\boldsymbol{u_d}, \boldsymbol{\tau}_d, \sigma_1, \sigma_2)$$

subject to

reduced forced discrete equations of motions during the contact phase for $n = 1, \ldots, \kappa$

$$\boldsymbol{P}_c^T(\boldsymbol{q}_n) \cdot \boldsymbol{P}^T(\boldsymbol{q}_n) \cdot \left[D_2 L_d(\boldsymbol{q}_{n-1}, \boldsymbol{q}_n) + D_1 L_d(\boldsymbol{q}_n, \boldsymbol{q}_{n+1}) + \boldsymbol{f}_{n-1}^+ + \boldsymbol{f}_n^- \right] = \boldsymbol{0} \tag{14}$$

$$\boldsymbol{g}_S(\boldsymbol{q}_{n+1}) = \boldsymbol{0}$$

reduced forced discrete equations of motions during the flight phase $n = \kappa + 1, \ldots, N-1$

$$\boldsymbol{P}^T(\boldsymbol{q}_n) \cdot \left[D_2 L_d(\boldsymbol{q}_{n-1}, \boldsymbol{q}_n) + D_1 L_d(\boldsymbol{q}_n, \boldsymbol{q}_{n+1}) + \boldsymbol{f}_{n-1}^+ + \boldsymbol{f}_n^- \right] = \boldsymbol{0}$$

boundary conditions

$$\boldsymbol{h}_{1d}(\boldsymbol{q}_0, \boldsymbol{p}_0) = \boldsymbol{0} \qquad h_{4d}(\boldsymbol{q}_N) < 0$$

path constraints for $n = 2, \ldots, N$

$$h_{2d}(\boldsymbol{q}_n) = 0 \qquad h_{3d}(\boldsymbol{q}_n) < 0$$

path constraints

for $n = 1, \ldots, \kappa - 2$	for $n = \kappa - 1$	for $n = \kappa + 1, \ldots, N$
$\lambda_{S_n}^3 < 0$	$\lambda_{S_{\kappa-1}}^3 = 0$	$g_S(\boldsymbol{q}_n) > 0$
$\sigma_{LB} < \sigma_1 < \sigma_{OB}$		$\sigma_{LB} < \sigma_2 < \sigma_{OB}$

the last inequalities ensure that the time steps $\sigma_1 \Delta t$ during the contact phase and $\sigma_2 \Delta t$ during the flight phase do not degenerate too small or large. This also yields a lower and upper bound on the total manoeuvre time. An additional equality constraint could be used to ensure a particular prescribed total manoeuvre time, however this is not imposed for the considered example.

7.1. Numerical Example

The initial guess for the optimal control problem takes place in the time interval $[0, 0.3]$ s. It uses $N = 24$ constant time steps and contact release takes place at the node number $N_\kappa = 18$. The motion starts at rest, the position of the upper part of the body is given by $\boldsymbol{\varphi}_0^1 = [0, 0, 0.8]$ m and the foot is fixed in $\boldsymbol{x}_S = [0, 0, 0]$ m. The initial guess for the discrete generalised configurations results from the forward dynamics simulation with a constant knee actuation $\tau_S^3 = 250$ Nm. The actuation torques of the initial guess are

set to zero and the discrete objective function for the monopedal jumper reads

$$\tilde{J}_d(\boldsymbol{u}_d, \boldsymbol{\tau}_d, \sigma_1, \sigma_2) = \frac{1}{h_N} \sum_{n=0}^{N-1} (t_{n+1} - t_n) \boldsymbol{\tau}_n^T \cdot \boldsymbol{\tau}_n,$$

whereby the jump height h_N is defined to be the distance between the torso's centre of mass and the ground at the end of the manoeuvre. An inequality constraint $h_{4d}(\boldsymbol{q}_N) < 0$ ensures a minimum jump height of 1.4 m. The objective function is motivated by the specific cost of transport, which means that the control effort per jump height is minimised. The scaling parameters are bounded between $0.5 \leq \sigma_1, \sigma_2 \leq 1.5$. The restricted optimisation problem is solved in MATLAB by using the `sqp` algorithm in the `fmincon` function, which is part of the optimisation toolbox and the numerical accuracy is set to 10^{-8}.

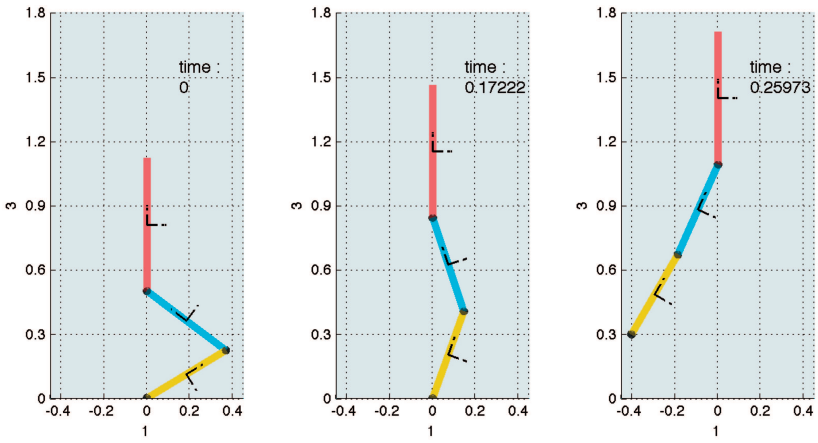

Fig. 11. Snapshots of the optimised motion at the beginning, the contact release and at the end of the motion

The optimisation algorithm computes a local minimum for which the objective function value is about $1.5202 \cdot 10^4 \ \frac{(Nm)^2\, s}{m}$ and a jump height of $h_N = 1.4\ m$ is achieved. The resulting jump height is just slightly above the prescribed minimal jump height, which illustrates the nonlinear relation between the control effort and the jump height in the cost function. The optimiser shortens the contacts phase using the scaling parameter $\sigma_1 = 0.9879$ and extends the flight time corresponding to $\sigma_2 = 1.2708$. The optimised motion of the monopedal jumper takes place in time interval $[0, 0.3217]\ s$, thus the total jumping time is reduced by 7.2333% in comparison to the initial guess. Figure 11 depicts three characteristic configurations, namely the initial and final configuration and the contact release at $t_k = 0.2099\ s$.

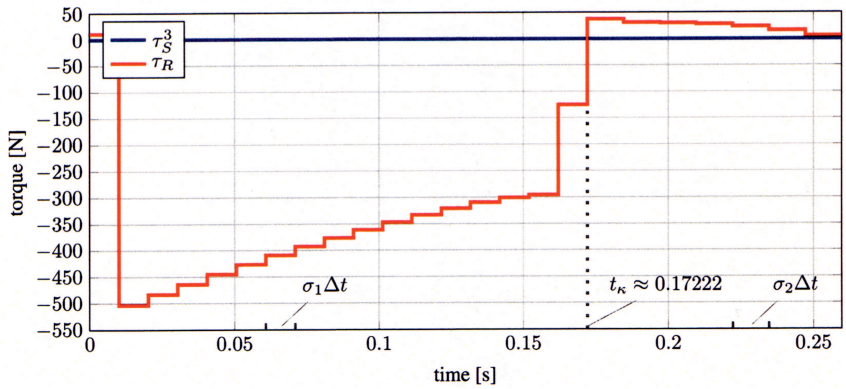

Fig. 12. Evolution of the discrete torques acting in the hip (third component τ_S^3 being responsible for the rotation in the plane) and in the knee (τ_R) of the monopedal jumper

In Figure 12, the actuation torques are plotted over the time and as a result of the optimisation, whereby the actuation of the revolute joint dominates. The torque evolution of the knee joint illustrates the essential effect of the contact phase for the whole jumping motion. The comparison between the actuation torques at the knee joint and the third component of the contact Lagrange multiplier (illustrated in Figure 13a)) shows that they are related during the contact phase as expected. The distance between the foot and the ground plane is depicted in Figure 13 b).

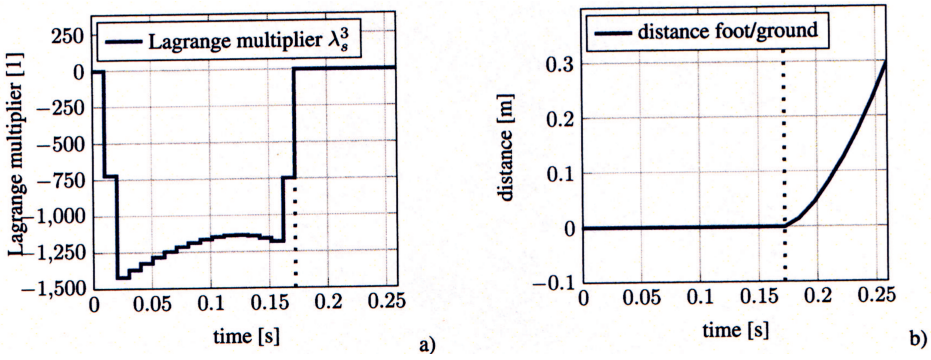

Fig. 13. In a) the evolution of the third component of the contact Lagrange multiplier is plotted over the time and b) illustrates the distance between the foot and the $(\boldsymbol{e}_1, \boldsymbol{e}_2)$-plane

8. Conclusion

This work investigates a variational integrator with structure preserving properties. The simple example of a monopedal jumper is used to discuss the theory of perfectly elastic, respectively perfectly plastic contact formulations.

The contact formulations are covered in forward dynamics simulations and in case of the perfectly elastic contact, the algorithm determines the contact time, the contact configuration and force. If the contact is modelled as perfectly plastic, the foot is fixed at the ground until the contact force changes the algebraic sign. Also here, the algorithm determines the corresponding contact release time and configuration. Further, the variational integrator and the formulations of the perfectly plastic contact are used in a direct transcription method to solve the optimal control problem with variable time step of a monopedal high jump. Therefore, two scaling parameters are used to optimise the contact and flight phase and as a result, the jumping motion is not artificially restricted.

Manuscript received by Editorial Board, September 27, 2012;
final version, November 11, 2012.

REFERENCES

[1] Aoustin Y., Formalskii A.: Upward Jump of a Biped. Proceedings of the Multibody Dynamics 2011, ECCOMAS Thematic Conference, 4-7 July 2011, USB, Brussels, Belgium.
[2] Betsch P., Steinmann P.: Constrained integration of rigid body dynamics. Comput. Methods Appl. Mech. Engrg., 2001, Vol. 191, pp. 467-488.
[3] Betsch P.: The discrete null space method for the energy consistent integration of constrained mechanical systems Part I: Holonomic constraints. Computer Methods in Applied Mechanics and Engineering, 2005, Vol. 194, pp. 5159-5190.
[4] Betsch P., Leyendecker S.: The discrete null space method for the energy consistent integration of constrained mechanical systems. Part II: Multibody dynamics. Int. J. Numer. Meth. Engrg, 2006, Vol. 67, pp. 499-552.
[5] Djoudi D., Chevallereau C., Aoustin Y.: Optimal reference motions for walking of a biped robot. Robotics and Automation, Proceedings of the 2005 IEEE International Conference, pp. 2002-2007.
[6] Fetacau R.C., Marsden J.E., Ortiz M., West M.: Nonsmooth Lagrangian Mechanics and Variational Collision Integrators. Siam J. Applied Dynamical Systems, 2003, Vol. 2, No. 3, pp. 381-416.
[7] François C., Samson C.: Energy Efficient Control of Running Legged Robots. A Case Study: The Planar One-Legged Hopper. Simulation et optimisation de systèmes complexes, Project ICARE, 1996, No. 3027.
[8] Gross D., Hauger W., Schnell W., Schröder J.: Technische Mechanik. Band 3: Kinetik. Springer, Berlin, Heidelberg, 2004.
[9] Kassat G.: Biomechanik für Nicht-Biomechanker. Fitness-Contur-Verlag, Rödinghausen, 1993.
[10] Kraft D.: On converting optimal control problems into nonlinear programming problems. Computational Mathematical Programming, 1985, Vol. F15, pp. 261-280.
[11] Koch M.W., Leyendecker S.: Structure preserving simulation of compass gait and monopedal jumping. Proceedings of the Multibody Dynamics 2011, ECCOMAS Thematic Conference, 4-7 July 2011, USB, Brussels, Belgium.
[12] Koditschek D E., Buehler M.: Analysis of a Simplified Hopping Robot. International Journal of Robotics Research, 1991, Vol. 10, pp. 587-605.

[13] Leyendecker S., Marsden J.E., Ortiz M.: Variational integrators for constrained dynamical systems. ZAMM, 2008, Vol. 88, No. 9, pp. 677-708.
[14] Leyendecker S., Ober-Blöbaum S., Marsden J.E., Ortiz M.: Discrete mechanics and optimal control for constrained systems. Optimal Control Applications & Methods, 2009, Vol. 31, pp. 505-528.
[15] Leyendecker S., Hartmann C., Koch M.W.: Variational collision integrator for chains. J. Comput. Phys., 2012, DOI 10.1016/j.jcp.2012.01.017, Vol. 231, p. 3896-3911.
[16] Marsden J.E., West M.: Discrete mechanics and variational integrators. Acta Numerica, 2001, Vol. 10, pp. 357-514.
[17] Roussel L., Candas-de Wit C., Goswami A.: Generation of energy optimal complete gait cycles for biped robots. Proceedings IEEE Conf. on Robotics and Automation, 1998.
[18] Stryk O., Bulirsch R.: Direct and indirect methods for trajectory optimization. Annals of Operations Research, 1992, pp. 357-373.
[19] Vaughan C.L., Davis B.L., O'Connor J.C.: Dynamics of Human Gait (Second Edition). Human Kinetics Book, Kiboho Publishers, Cape Town, 1992.

Symulacja skoku jednonożnego z zachowaniem struktury

S t r e s z c z e n i e

Środowisko człowieka składa się z bardzo wielu różnorodnych systemów mechanicznych i biomechanicznych, w których mogą wystąpić różne typy kontaktów. W przedstawionej pracy rozważa się jednonożnego skoczka modelowanego jako trójwymiarowe ciało sztywne z kontaktem i symuluje się jego dynamikę metodą, w której zachowana jest struktura systemu. W zastosowanym integratorze mechanicznym wykorzystano wersję zasady Lagrange-d'Alemberta z ograniczeniami. Wynikający stąd integrator wariacyjny zachowuje symplektyczność i mapę momentów pędu dynamiki układu wieloczłonowego. Aby zapewnić zachowanie struktury i poprawność geometryczną, w rozwiązaniu tego problemu nie stosowano wygładzania. Wyznaczono konfigurację kontaktów, czas i siłę, zamiast polegać na aproksymacji zagadnienia kontaktu z wygładzeniem poprzez potencjał kary. Poza sformułowaniem niewygładzonego zagadnienia symulacji w dynamice prostej, przedmiotem zainteresowania autorów jest także optymalne sterowanie skoku wzwyż skoczka jednonożnego. Zagadnienie sterowania optymalnego zostało rozwiązane przy użyciu metody transkrypcji bezpośredniej przekształcającej ten problem w zagadnienie optymalizacji z ograniczeniami – patrz [14].